May 17th, 11:15 AM

LIDAR Measurements of Free-surface Profiles and Turbulent Scales in a Hydraulic Jump

Laura Montano
University of New South Wales, l.montano@wrl.unsw.edu.au

Stefan Felder
University of New South Wales

Recommended Citation

Montano, Laura (2018). LIDAR Measurements of Free-surface Profiles and Turbulent Scales in a Hydraulic Jump. Daniel Bung, Blake Tullis, 7th IAHR International Symposium on Hydraulic Structures, Aachen, Germany, 15-18 May. doi: 10.15142/T3Q64F (978-0-692-13277-7).

7th International Symposium on Hydraulic Structures Aachen, Germany, 15-18 May 2018
ISBN 978-0-692-13277-7 DOI: 10.15142/T3Q64F

LIDAR measurements of free-surface profiles and turbulent scales in a hydraulic jump

L. Montano[1] & S. Felder[1]
[1]*Water Research Laboratory, School of Civil and Environmental Engineering, UNSW Sydney, Manly Vale, Australia*
E-mail: l.montano@wrl.unsw.edu.au

Abstract: *Hydraulic jumps are complex turbulent phenomena characterized by a rapid transition from fast shallow flows to slow deep flows. Strong energy dissipation, air entrainment and large-scale turbulence are some of the key features of hydraulic jumps. The understanding of the free-surface characteristics is limited. Previous experiments have been conducted with pointer gauges, wire gauges and acoustic displacement meters limiting the measurements to a fixed point per sensor along the surface of the hydraulic jump. Recent experiments with a LIDAR measured a continuous and time-varying free-surface profile of an aerated hydraulic jump providing basic statistical free-surface properties. The present study investigated more advanced parameters including the turbulent characteristics of the free-surface in a fully aerated hydraulic jump. Auto- and cross-correlation analyses were performed along the hydraulic jump and the auto- and cross-correlation time scales were calculated. An integration of the maximum correlation coefficients along the hydraulic jump provided the longitudinal free-surface integral turbulent length scales. The comparison with previous studies showed turbulent scales of the same order of magnitude. The turbulent scales in the present study exceeded past results which may be linked with the extended integration range due to the high resolution of measurement points along the hydraulic jump. The present study presented the most spatially detailed description of the turbulent free-surface characteristics in hydraulic jumps to date, including the turbulent free-surface scales in the jump toe region. Further research is needed to identify the effects of instrumentation and raw signal filtering on the free-surface integral scales.*

Keywords: *Hydraulic jumps, LIDAR, free-surface fluctuations, jump toe oscillations, integral turbulent scales.*

1. Introduction

A hydraulic jump is a rapidly varied flow phenomenon occurring in the transition from fast supercritical to slow subcritical flows. A hydraulic jump is characterized by three-dimensional motions, turbulence and energy dissipation. During the last century, extensive research has been conducted to understand the complex behavior in hydraulic jumps including conjugate depth relationship, energy dissipation, air-water flow properties and characterization of the free-surface. Previous studies measured the average free-surface profiles of the hydraulic jump with pointer gauges (e.g. Rouse et al. 1959; Rajaratnam 1962; Hager 1993), with wire gauges (e.g. Mouaze et al. 2005; Murzyn et al. 2007) and with Acoustic Displacement Meters (ADM) (e.g. Kucukali and Chanson 2008; Murzyn and Chanson 2009; Chachereau and Chanson 2011; Wang and Chanson 2015). These instruments provided the free-surface profiles based on single fixed point measurements along the hydraulic jump. Recently Montano et al. (2018) measured the time varying free-surface profile of a hydraulic jump with a Light Detection and Ranging Instrument (LIDAR), measuring instantaneous and continuous time-varying free-surface profiles for the first time.

Typical analyses of the free-surface characteristics in hydraulic jumps comprise the estimation of the time-averaged free-surface profiles (e.g. Bakhmeteff and Matzke 1936; Rajaratnam 1962; Hager 1993; Montano et al. 2018)), the observations of the free-surface fluctuations (e.g. Mouaze et al. 2005; Murzyn et al. 2007; Murzyn and Chanson 2009; Chachereau and Chanson 2011; Montano et al. 2018) and the analysis of the characteristic frequencies of the free-surface fluctuations (e.g. Murzyn and Chanson 2009; Chachereau and Chanson 2011; Wang 2014; Montano et al. 2018). More advanced free-surface properties are the free-surface integral turbulent time and length scales. Simultaneous sampling at defined longitudinal distances along the hydraulic jump and the auto-correlation and cross-correlation analyses of the simultaneous signals can provide information about the sizes of the longitudinal turbulence structures (Mouaze et al. 2005; Murzyn et al. 2007; Chachereau and Chanson 2011). Past studies calculated the free-surface integral turbulent scales based upon measurements with wire gauges (Mouaze et al. 2005; Murzyn et al. 2007), with ADMs (Chachereau and Chanson 2011; Wang and Murzyn 2016) and with high-speed cameras (Mouaze et al. 2005). These experiments provided the characteristic free-surface turbulent time and length scales showing an increase in length scales with increasing distance from the jump toe (Murzyn et al. 2007; Chachereau and Chanson 2011). The experiments and subsequent analyses were conducted for single point measurements at defined distances between two instruments, and the results were affected by the jump toe oscillation as reported by Mouaze et al. (2005). Herein, the present study investigated the integral turbulent scales of the free-surface in an aerated hydraulic jump based upon the

time-varying free-surface profiles measured with a LIDAR. The present study provided new insights into the characteristic turbulent scales in a hydraulic jump. The results highlighted the effects of the jump toe oscillations on the turbulent scales near the jump toe and provided a continuous integral turbulent scale distribution along the hydraulic jump.

2. Methodology

Experiments were performed in a rectangular flume of 40 m length, 0.6 m width and 0.6 m height at UNSW's Water Research Laboratory. The channel had glass walls and the floor was made of painted compressed fibrous cement. The hydraulic jump was generated downstream of an inbuilt sloped channel section made of smooth plywood with a slope of 5 degrees. A sharp-crested weir located at the downstream end of the flume controlled the hydraulic jump location. Supercritical and fully developed flow conditions were obtained at the downstream end of the sloped section as confirmed in detailed measurements with a Pitot tube (Montano and Felder 2017). The discharge was controlled with an ABB® WaterMaster FET100 electromagnetic flowmeter with an accuracy of 0.4%. Conjugate flow depths upstream and downstream of the hydraulic jump were measured with a pointer gauge. The free-surface characteristics of the aerated hydraulic jump were measured with a LIDAR. The LIDAR was located 1 m upstream of the average hydraulic jump toe position and approximately 1.5 m above the channel bed. The LIDAR was carefully oriented to record the free-surface characteristics in channel centerline.

A LIDAR is a laser measurement sensor which is based on the Time of Flight Principle, i.e. the estimation of the travel time between a surface and the LIDAR (Blenkinsopp et al. 2012; SICK 2015). In the present study, an industrial LIDAR, SICK LMS511 was used with an angular scanning step of 0.25 degrees and a scanning frequency of 35 Hz. Continuous data were recorded for 1 hour. The technical specifications by the manufacturer indicated a standard resolution larger than ±2.5 cm (SICK 2015). Previous laboratory studies of breaking waves with identical or similar LIDAR instruments (LMS511 and LMS200) identified a LIDAR accuracy of about 6 mm compared with wave resistance probes validating the use of LIDARs in aerated flows (Blenkinsopp et al. 2012; Streicher et al. 2013; Damiani and Valentini 2014). In the present study, the LIDAR was applied in a fully-aerated hydraulic jump to optimize the detection of the free-surface (Note that the LIDAR was unable to measure the free-surface of clear water). A Hampel identifier method was used to filter water splashes and droplets observed in the raw signal data. Once the raw signal was filtered, the free-surface profiles were linearly interpolated to obtain an unified grid with a resolution of less than 1 cm steps in x-direction. The present experiments were conducted with a flow depth upstream of the hydraulic jump d_1 = 0.032 m, a flow rate of Q = 0.050 m^3/s, an upstream Froude number Fr_1 = 4.7 and a Reynolds number Re = 8.4x10^4. Further details of the experimental setup and the flow conditions were presented in Montano and Felder (2017), Li et al. (2017) and Montano et al. (2018).

In the present study, the LIDAR recorded continuous and time-varying free-surface profiles in a hydraulic jump with a freely oscillating jump toe. The analysis of the raw free-surface profiles comprised basic statistical analyses yielding the mean free-surface profiles and the standard deviation of the free-surface fluctuations. Advanced auto- and cross-correlation analyses provided the longitudinal free-surface integral time and length scales. The auto-correlation time scales T_{xx} represented a characteristic longitudinal advective time at every measurement location along the hydraulic jump. T_{xx} was calculated based upon the raw free-surface signal at a given location following the approach by Chachereau and Chanson (2011):

$$T_{xx} = \int_{\tau=0}^{\tau=\tau(R_{xx}=R_{xx,min}||R_{xx}=0)} R_{xx}(\tau) d\tau \quad (1)$$

where τ is the time lag, R_{xx} is the auto-correlation function of the raw signal at a given position and $R_{xx,min}$ is the minimum auto-correlation coefficient. The corresponding cross-correlation time scales T_{xy} were calculated between two simultaneously sampled measurement points with known longitudinal separation distance Δx (Chachereau and Chanson 2011) using:

$$T_{xy} = \int_{\tau=\tau(R_{xy}=R_{xy,max})}^{\tau=\tau(R_{xy}=R_{xy,min}||R_{xy}=0)} R_{xy}(\tau) d\tau \quad (2)$$

where R_{xy} is the cross-correlation function and $R_{xy,min}$ and $R_{xy,max}$ are the minimum and maximum cross-correlation coefficients respectively. Both auto- and cross-correlation time scales were calculated based upon an integration of the correlation function from the maximum correlation coefficient to the first crossing with the x-axis. When the correlation function did not cross the x-axis, $R_{xx,min}$ and $R_{xy,min}$ respectively were selected as the integration limits.

The integration of the maximum cross-correlation coefficient $R_{xy,max}$ from $\Delta x = 0$ to a maximum longitudinal distance between two sampling points Δx_{max}, where $R_{xy,max}$ was small, provided the streamwise free-surface integral turbulent length scales L_{xy} (Murzyn et al. 2007; Chachereau and Chanson 2011) using:

$$L_{xy} = \int_{\Delta x=0}^{\Delta x=\Delta x_{max}} R_{xy,max}(x)dx \quad (3)$$

The free-surface integral turbulent length scales represented a characterization of the large free-surface motions interacting in the streamwise direction. Note that the selection of the most appropriate value of $R_{xy,max}$ and the corresponding distance Δx_{max}, is discussed in Section 5.

The LIDAR provided a spatially detailed representation of the time-varying free-surface profiles allowing the cross-correlation analysis between simultaneously sampled data points along the centerline of the hydraulic jump. To identify any inherent correlation of the LIDAR signals, the raw data signal of the LIDAR of the channel bed without water was used. The cross-correlation of these signals showed an asymptotic positive self-correlation value $R_{xy,min}$ = 0.0667. To avoid any instrument-specific positive correlation in the calculation of the turbulent length scales, the LIDAR self-correlation value $R_{xy,min}$ = 0.0667 was subtracted from the auto- and cross-correlation functions. No additional filtering process was implemented and further research is required to check if low pass filtering is required to remove the slow longitudinal motions of the hydraulic jump as was conducted in the analysis of Chachereau and Chanson (2010).

3. Basic Free-surface Characteristics

The LIDAR recorded the time-varying free-surface profile of the hydraulic jump. A typical sample of 25 free-surface profiles with a time step of 0.4 s is shown in Figure 1. The profiles are shown in dimensionless terms d/d_1 along the hydraulic jump x/d_1 where d is the flow depth and x is the distance along the hydraulic jump (Figure 1). The time step of 0.4 s corresponded to a frequency of 2.5 Hz which represented a typical characteristic frequency of the free-surface fluctuations in hydraulic jumps (Murzyn and Chanson 2009; Chachereau and Chanson 2011; Wang 2014; Montano et al. 2018). The free-surface profiles in Figure 1 highlighted the capability of the LIDAR to record the temporal and spatial variations of the free-surface in aerated hydraulic jumps. Figure 1 also shows the minimum and maximum free-surface profiles of the 25 individual profiles as well as the minimum and maximum free-surface profiles for the complete sampling duration in the present study. The large differences in maximum and minimum free-surface profiles highlighted the strong free-surface fluctuations of the hydraulic jump as well as the strong longitudinal movements of the jump roller. For the 25 profiles, the dimensionless jump toe positions varied from $-2.5 < x/d_1 < 1.58$. For the full sampling duration of 1 hour, the hydraulic jump movements increased significantly to $-6.3 < x/d_1 < 6.5$. The strong jump toe oscillations highlighted that the longitudinal movements of the hydraulic jump should be taken into account for the characterization of the free-surface features in hydraulic jumps.

A statistical analysis of the basic free-surface characteristics of the hydraulic jump was conducted providing the mean, median and standard deviation of the free-surface profiles (Figure 1). A clear difference in the mean and median free-surface profiles was observed for $-3 < x/d_1 < 2$ with a maximum difference of 25% for $x/d_1 = 0$. Further downstream for $x/d_1 > 2$, the mean and median profiles differed less than 2%. The differences in mean and median profiles close to the jump toe were linked with the longitudinal movement of the jump toe highlighting the need to incorporate the jump toe oscillations into the analysis of the free-surface properties as was reported in Montano et al. (2018). The dimensionless standard deviation profiles d'/d_1 are also shown in Figure 1, showing a sharp increase in the standard deviation from $d'/d_1 = 0$ at $x/d_1 = -5.20$ to a maximum peak of about $d'/d_1 = 0.7$ at $x/d_1 = 2.41$. For $2.41 < x/d_1 < 23.5$, the dimensionless standard deviation decreased gradually with a slope > 2% followed by a slower decrease of 0.8% approximately for $x/d_1 > 23.5$. This result suggested that the fluctuation pattern stabilized at $x/d_1 > 23.5$ which corresponded to the end of the roller section of the hydraulic jump.

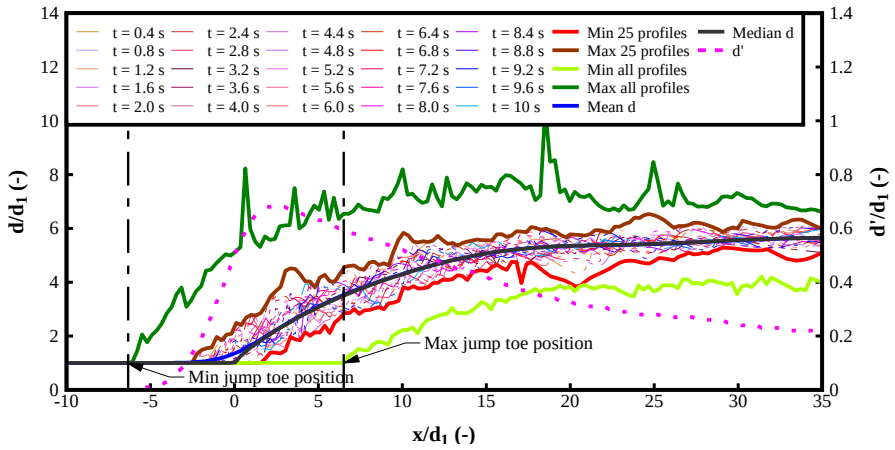

Figure 1. Time-varying free-surface profiles and basic statistical results in a fully aerated hydraulic jump measured with a LIDAR: Q = 0.050 m^3/s, d_1 = 0.032 m, Fr_1 = 4.7, Re = 8.4x10^4; Time step of *0.4* s between profiles.

The strong longitudinal movements of the hydraulic jump coincided with strong fluctuations of the free-surface. Figure 2 shows the normalized amplitude Λ of the free surface profiles for the complete sampling time along the hydraulic jump between $-7 < x/d_1 < 35$. The normalized amplitude was defined as the difference between the maximum and minimum free-surface profiles divided by d_1 over the sampling duration. Albeit some scatter, the maximum amplitude was observed for $0 < x/d_1 < 7$ with $\Lambda > 5$ which appeared to be associated with the jump toe oscillations. Large amplitudes were also observed for $7 < x/d_1 < 14$ corresponding to the roller section of the hydraulic jump. For $x/d_1 > 14$, at the downstream end of the roller, Λ showed a gradual decrease associated with reduced free-surface fluctuations. An almost constant amplitude value of $\Lambda = 3$ was observed at $x/d_1 > 23$ associated with the conjugate depth region of the hydraulic jump. The present results were consistent with the free-surface observations in previous experiments (Li et al. 2017; Montano et al. 2018). The amplitude along the hydraulic jump was well correlated with (R = 0.91):

$$\Lambda = \frac{4.345+0.695\left(\frac{x}{d_1}\right)}{1+0.055\left(\frac{x}{d_1}\right)+0.0067\left(\frac{x}{d_1}\right)^2} \qquad \text{for } x/d_1 > -6 \tag{4}$$

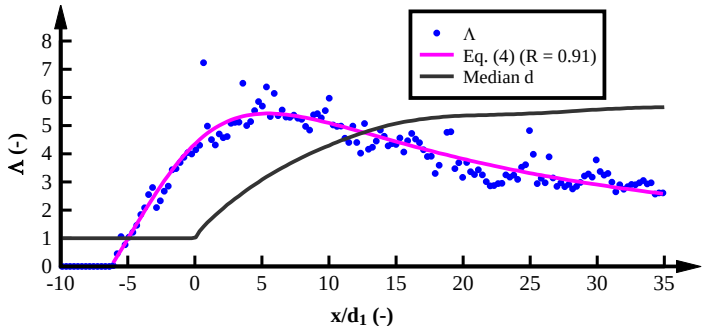

Figure 2. Distribution of the maximum amplitude of the minimum and maximum free-surface profiles measured with a LIDAR: Q = 0.050 m^3/s, d_1 = 0.032 m, Fr_1 = 4.7, Re = 8.4x10^4; Comparison with best fit function (Eq. 4) and median profile.

A qualitative comparison between the amplitudes for 25 profiles (Figure 1) and 121,386 profiles (Figure 2) showed a similar trend in the amplitudes with larger amplitudes near the jump toe. However, the amplitude values observed for the complete analysis (Figure 2) was almost twice the amplitude observed for the smaller interval (Figure 1). This result highlighted the influence of the sampling time on the analysis of the free-surface features in hydraulic jumps. Further research is required to identify the minimum sampling time needed for a complete analysis of the free-surface properties.

4. Advanced Free-surface Characteristics

4.1. Auto- and Cross-correlation Time Scales

The auto-correlation time scale T_{xx} represented the advective time of the turbulent free-surface structures. Auto-correlation time scales in air-water flows in hydraulic jumps has been reported previously (Wang et al. 2014) and the present study expanded the approach to the free-surface (Figure 3). Figure 3a illustrates typical auto-correlation functions near the jump toe and Figure 3b shows the dimensionless auto-correlation free-surface time scales $T_{xx}(g/d_1)^{0.5}$ as a function of the distance from the mean jump toe x/d_1. The percentage of non-detected data points measured with the LIDAR is added in Figure 3b. Large auto-correlation time scales of up to $T_{xx}(g/d_1)^{0.5} \approx 4$ were observed between $2.5 < x/d_1 < 2$ corresponding to $T_{xx} \approx 0.25$ s. The large time scales were observed within the range of the maximum and minimum jump toe oscillations (Figure 1) and are the result of the large auto-correlation coefficients close to the jump toe (Figure 3a). Typical auto-correlation functions near the jump toe position showed that $R_{xx} > 0$ for $-3.15 \leq x/d_1 \leq 2.11$ (Figure 3a) with minimum $R_{xx} > 0.1$ for $x/d_1 > -2.3$. The integration of the auto-correlation functions to the minimum value of R_{xx} (with $R_{xx} > 0.1$) resulted in large correlation time scales near the jump toe. It is acknowledged that such large time scales may be suspicious and that a low-pass filtering could shift the correlation function downwards reducing the corresponding time scales. In the present study, the data were presented without filtering to highlight the strong effect of the jump toe oscillations on the auto-correlation functions and the integral free-surface time and length scales.

The peak values of $T_{xx}(g/d_1)^{0.5}$ were observed at the mean jump toe position $x/d_1 = 0$. Upstream and downstream of this position, the auto-correlation time scales increased/decreased rapidly (Figure 3b). Downstream of the region affected by the jump toe oscillations, the integral time scales remained almost constant $T_{xx}(g/d_1)^{0.5} \approx 1$ for $x/d_1 > 5$. The corresponding dimensional auto-correlation time scales $T_{xx} \approx 0.05$ s were similar to the corresponding air-water flow auto-correlation time scale of $T_{xx} \approx 0.03$ to 0.05 s (Wang 2014). For $x/d_1 > 17$, the auto-correlation time scales increased slightly possibly related to the increase in the percentage of non-detected data points (Figure 3b).

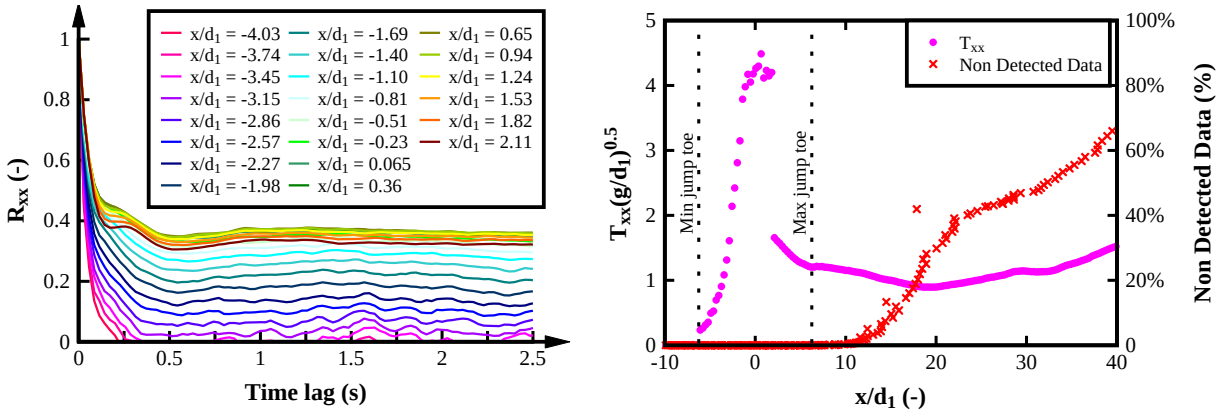

a) Auto-correlation functions near the jump toe for $-4.03 < x/d_1 < 2.11$

b) Auto-correlation time scales along the hydraulic jump; "x" = percentage of Non Detected Data points.

Figure 3. Auto-correlation functions and integral time scales in a hydraulic jump measured with a LIDAR: $Q = 0.050$ m^3/s, $d_1 = 0.032$ m, $Fr_1 = 4.7$, $Re = 8.4 \times 10^4$

The cross-correlation time scale T_{xy} provided a measure of the longitudinal coherent free-surface structures of the hydraulic jump based on the distance between two points of known distance (Chachereau and Chanson 2010; Wang 2014). While the auto-correlation time scales were calculated for a single point location, the cross-correlation time scales were calculated for a range of distances Δx. Figure 4 shows the dimensionless cross-correlation time scales $T_{xy}(g/d_1)^{0.5}$ as a function of $\Delta x/d_1$ between a fixed point of analysis $(x/d_1)_0$ and the cross-correlated points with various downstream distances $\Delta x/d_1$. The analysis was conducted for 110 measurement points along the hydraulic jump. The LIDAR delay between two adjacent points of analysis ($\Delta x \approx 1$ cm) was smaller than 4×10^{-5} s and was considered negligible. However, further research with higher sampling rates is required to identify the impact of the LIDAR delay on the cross-correlation time scales.

For all starting points of the cross-correlation analyses, Figure 4 shows that $T_{xy}(g/d_1)^{0.5}$ declined with increasing distance between correlated data points $\Delta x/d_1$. This pattern was observed for different regions along the hydraulic jump. The correlation time scale for $\Delta x/d_1 = 0$ corresponded to the auto-correlation time scale (Figure 3). Likewise, the curve of $T_{xy}(g/d_1)^{0.5}$ at different $(x/d_1)_0$ was strongly influenced by the initial time scale value, i.e. $T_{xx} = T_{xy}$. In Figure 4, four distinct regions are shown reflecting different patterns of $T_{xy}(g/d_1)^{0.5}$. While Figure 4 shows only four points of analysis per region, the behavior of all curves in a region was similar. In the region upstream of the mean jump toe location, $3.73 < (x/d_1)_0 < -0.81$, $T_{xy}(g/d_1)^{0.5}$ increased with an increase in $(x/d_1)_0$ (Figure 4a) which was consistent with the increase in the auto-correlation functions and time scales (Figure 3). For a region close to the mean jump toe (Figure 4b), $-0.52 < (x/d_1)_0 < 0.94$, the cross-correlation time scale was large, $T_{xy}(g/d_1)^{0.5} > 1$ at $\Delta x/d_1 = 10$ with similar patterns and similar values for different locations $(x/d_1)_0$. This region showed the largest dimensionless cross-correlation time scales along the hydraulic jump. This observation suggested the largest coherence of the longitudinal turbulent free-surface structures of the hydraulic jump close to the mean jump toe $(x/d_1)_0 = 0$. Further downstream, for $2.70 < (x/d_1)_0 < 9.14$, $T_{xy}(g/d_1)^{0.5}$ decreased with an increase in $(x/d_1)_0$. For $9.43 < (x/d_1)_0 < 15$, the decline in $T_{xy}(g/d_1)^{0.5}$ with increasing $(x/d_1)_0$ was less pronounced in contrast to data further upstream highlighting a similar coherence between the turbulent structures at the end of the roller (Figure 4d).

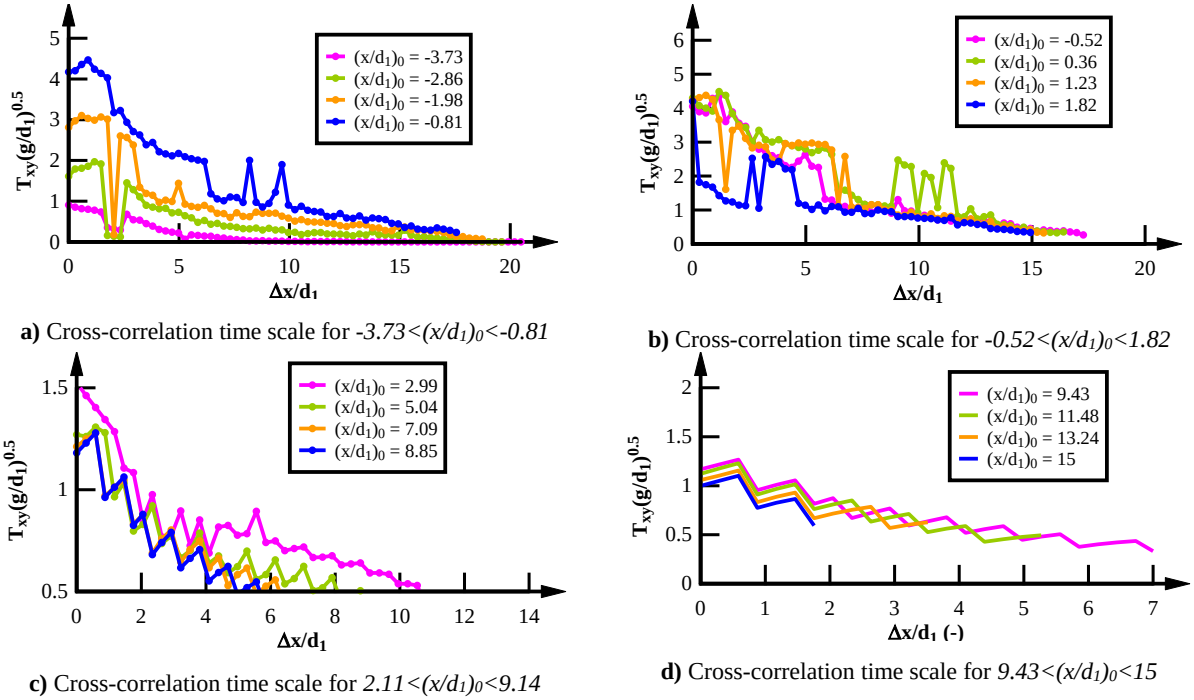

a) Cross-correlation time scale for $-3.73<(x/d_1)_0<-0.81$

b) Cross-correlation time scale for $-0.52<(x/d_1)_0<1.82$

c) Cross-correlation time scale for $2.11<(x/d_1)_0<9.14$

d) Cross-correlation time scale for $9.43<(x/d_1)_0<15$

Figure 4. Dimensionless cross-correlation integral free-surface time scales in a hydraulic jump measured with a LIDAR: Q = 0.050 m^3/s, d_1 = 0.032 m, Fr_1 = 4.7, Re = 8.4x10^4

4.2. Integral Free-Surface Length Scales

The maximum cross-correlation coefficient $R_{xy,max}$ provided the longitudinal correlation between two points of analysis. Figure 5a shows typical values of $R_{xy,max}$ as function of the normalized dimensionless separation distance $(\Delta x/d_1)/(\Delta x/d_1)_{30}$, where $(\Delta x/d_1)_{30}$ corresponded to $R_{xy,max} = 0.3$ following the approach by Chachereau and Chanson (2011). Figure 5a includes the present LIDAR data and ADM data from Chachereau and Chanson (2011). The present maximum cross-correlation coefficients showed good agreement with previous experimental data as well as the exponential decay reported by Chachereau and Chanson (2011):

$$R_{xy,max} = \exp\left(-1.204 \frac{\Delta x/d_1}{(\Delta x/d_1)_{30}}\right) \quad (5)$$

A good agreement of LIDAR data and Eq. (5) in particular was observed for $(\Delta x/d_1)/(\Delta x/d_1)30 < 1$. Further downstream for $(\Delta x/d_1)/(\ \Delta x/d_1)30 > 1$, the exponential decay was followed by a slight increase in the maximum correlation

coefficients associated with large data scatter and an increase of non-detected data points towards the downstream end of the roller. Despite the data scatter, Eq. (5) predicted the decay in maximum correlation coefficients well (Figure 5a). Figure 5b presents the $R_{xy,max}$ curves at different positions $(x/d_1)_0$ as function of the distance from the jump toe. For larger $(x/d_1)_0$, $R_{xy,max}$ shifted upwards showing stronger positive correlation. For $(x/d_1)_0 < 6.5$, a change in the slope of the curves was observed at $x/d_1 = 6.5$ corresponding to the region of the maximum jump toe oscillation. This result suggested a strong effect of the jump toe motions on the correlation functions for $(x/d_1)_0 < 6.5$. At $(x/d_1)_0 \approx 23$, $R_{xy,max}$ showed a minimum corresponding to the beginning of the conjugate flow depth region.

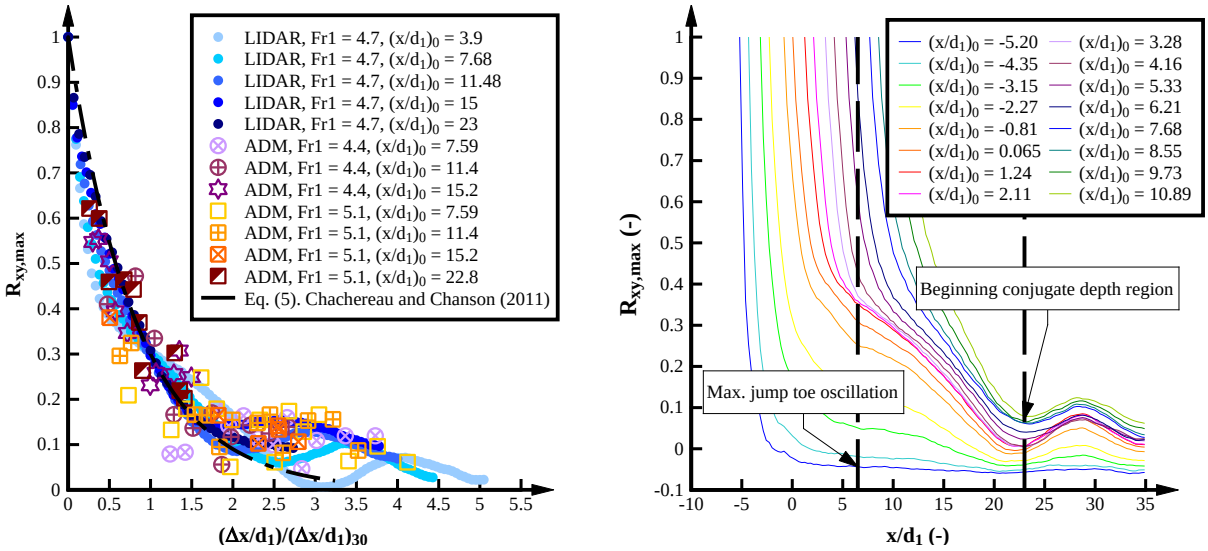

a) Maximum cross-correlation coefficients as function of the normalized dimensionless separation distance; Comparison with ADM data and Eq. (5) (Chachereau and Chanson 2011)

b) Maximum cross-correlation coefficients as function of the longitudinal distance from the mean jump toe

Figure 5. Maximum cross-correlation coefficients along a hydraulic jump measured with a LIDAR. $Q = 0.050$ m^3/s, $d_1 = 0.032$ m, $Fr_1 = 4.7$, $Re = 8.4$x10^5.

The integral free-surface length scales are a function of the maximum cross-correlation coefficients $R_{xy,max}$ integrated along the hydraulic jump (Eq. 3). The longitudinal free-surface length scales L_{xy} were calculated based upon the continuous free-surface signal of the LIDAR. Figure 6**Figure 6.** presents the dimensionless integral length scales L_{xy}/d_1 in the present study as a function of x/d_1. The present data are compared with previous studies including the study with ADMs by Chachereau and Chanson (2011) (Figure 6a) and wire gauges by Murzyn et al. (2007) (Figure 6b). For consistency with the previous studies, the maximum sensor separation distance Δx_{max} for the calculation of the integral length scales was conducted with constant separation values, i.e. $\Delta x_{max} = 0.23$ m for consistency with the study of Chachereau and Chanson (2011) (Figure 6a) and $\Delta x_{max} = 0.1$ m consistent with the study of Murzyn et al. (2007) (Figure 6b). Note that in the study of Murzyn et al. (2007), Δx_{max} was a function of $(x/d_1)_0$ (e.g. $\Delta x_{max} \neq 0.1$ m). However, the variation of Δx_{max} as function of $(x/d_1)_0$ was not reported and the maximum limit tested between the sensors was used as a reference ($\Delta x_{max} = 0.1$). Figure 6 shows also the median free-surface profile d/d_1 of the present hydraulic jump as well as the percentage of non-detected data points.

The LIDAR data analysis provided a continuous and detailed profile of the variation of L_{xy}/d_1 along the hydraulic jump (Figure 6). The integral length scales showed a strong monotonic increase until $x/d_1 = 1.24$ for $\Delta x_{max} = 0.23$ m and 0.1 m respectively (Figure 6a & b). This increase was consistent with the strong increase in auto- and cross-correlation functions close to the jump toe (Figure 3 & 4). The largest length scales were close to the jump toe which was consistent with the observation of largest auto- and cross-correlation time scales and largest standard deviations close to the jump toe. The findings highlighted the strong effects of the jump toe oscillations on the free-surface characteristics in hydraulic jumps. A slight decrease in the dimensionless length scale was observed between $1.24 < x/d_1 < 3.6$ followed by close to constant length scales further downstream suggesting similar interactions of the large longitudinal free-surface structures in the latter half of the hydraulic jump. Figure 6 also shows a significant increase of L_{xy} with the increase of Δx_{max} (while maintaining the overall distribution shape). Compared to the previous studies with ADMs and wire gauges, the integral length scales showed significantly larger integral length scales for $x/d_1 < 15$.

Further downstream, for $x/d_1 > 15$, the differences in L_{xy}/d_1 were small. The main differences were observed near the jump toe and in the first half of the jump roller, suggesting that the differences in the integral turbulent length scale observations may be linked with the jump toe oscillations. No low or high pass filter was applied in the present study and the slow and fast components of the jump toe movements were included in the cross-correlation functions. It is unclear if the constant inflow depth d_1 had an effect on the correlation functions. Additional experiments with simultaneous measurements of LIDAR and ADMs are recommended to identify the effect of jump toe oscillations on the integral free-surface time and length scales. This comparative study would also clarify potential effects of the instrumentation.

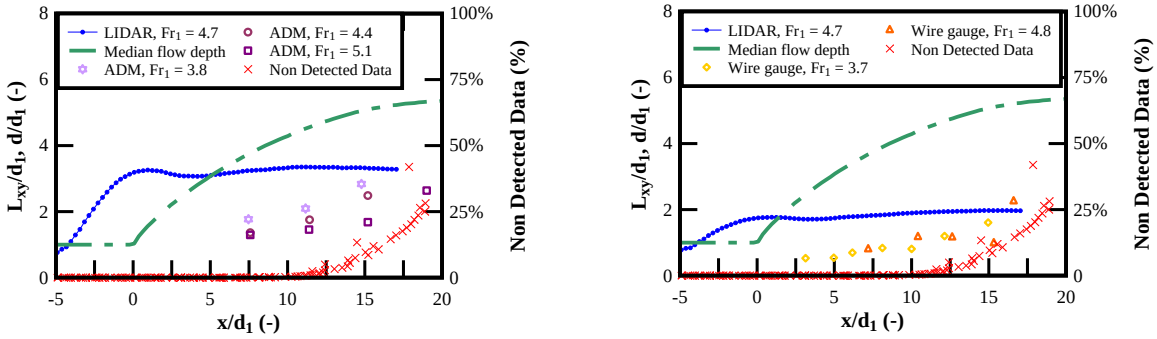

a) Integral free-surface length scale; comparison with ADM data of Chachereau and Chanson (2011); Analysis for Δx_{max} = 0.23 m

b) Integral free-surface length scale; comparison with wire gauge data of Murzyn et al. (2007); Analysis for Δx_{max} = 0.1 m

Figure 6. Dimensionless integral free-surface length scales in a hydraulic jump measured with a LIDAR: Q = 0.050 m^3/s, d_1 = 0.032 m, Fr_1 = 4.7, Re = 8.4x10^4; comparison with median flow depth, non-detected data points and previous studies

5. Discussion

The calculation of the integral length scales is a function of the maximum separation distance Δx_{max} between the sensors. Murzyn et al. (2007) showed that the correlation coefficients should be close to 0 for a specific separation distance between the sensors (Δx_{max}). The correlation analysis of the LIDAR data after the subtraction of the LIDAR self-positive correlation coefficient was positive for most of the hydraulic jump data suggesting a possibly infinite value of the integral length scales. Figure 7 shows typical distributions of $R_{xy,max}$ data in the present experiments for different longitudinal hydraulic jump positions $(x/d_1)_0$. Figure 7 shows the minimum $R_{xy,max}$ value in cases where the $R_{xy,max}$ curve did not cross the x-axis. For all data in the present study, $R_{xy,max}$ crossed the x-axis for $(x/d_1)_0 < 0$. For $(x/d_1)_0 > 0.65$, $R_{xy,max}$ was always positive with increasing minimum $R_{xy,max}$ values with increasing $(x/d_1)_0$. For correlation functions with positive values of $R_{xy,max}$, the selection of the minimum $R_{xy,max}$ value appeared to be the most meaningful upper integration limit for the calculation of the integral length scales (Eq. 3).

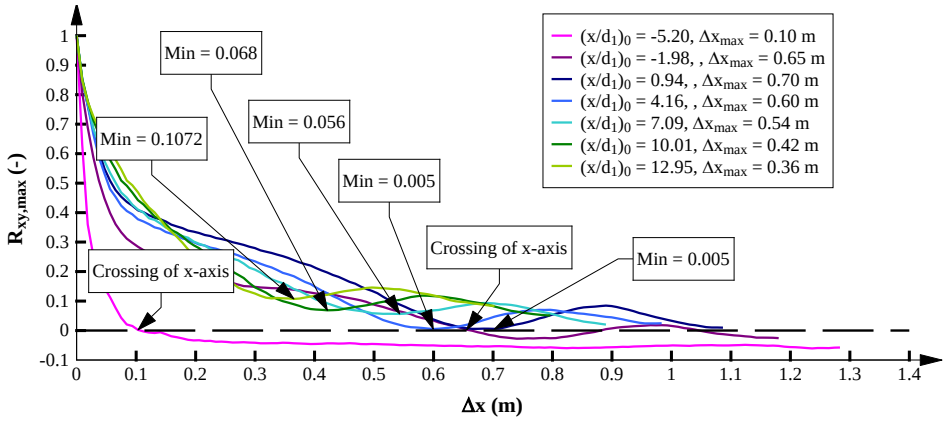

Figure 7. Maximum cross-correlation coefficients along the hydraulic jump.

Figure 8.a shows the variation of Δx_{max} and the minimum values of $R_{xy,max}$ as function of x/d_1. For $-4 \leq x/d_1 \leq 0$, Δx_{max} was almost constant ($\Delta x_{max} \approx 0.6$ m). For $x/d_1 > 0$, Δx_{max} decreased gradually from $\Delta x_{max} = 0.66$ at $x/d_1 = 0$ to $\Delta x_{max} = 0.3$ at $x/d_1 = 17$. Figure 8.a also shows the distribution of the minimum values of $R_{xy,max}$ as function of x/d_1. For $x/d_1 \leq 0$, the minimum values of $R_{xy,max}$ always crossed the x-axis while for $x/d_1 > 0$, the minimum values of $R_{xy,max}$ were always positive with increasing values with increasing distance from the jump toe.

Figure 8.b shows the distribution of the integral free-surface length scales as a function of x/d_1 including L_{xy} calculated with constant integration limits of $\Delta x_{max} = 0.10$ m and 0.23 m respectively and L_{xy} calculated based upon the minimum values of $R_{xy,max}$ ($L_{xy,min}$). For $x/d_1 < 0.94$, $L_{xy,min}$ increased with increases in x/d_1 which was in agreement with observations of L_{xy} calculated with constant integration limits. At $x/d_1 = 0.94$, the integral free-surface length scales were largest, $L_{xy,min} = 0.18$ m, linked with the jump toe oscillations. For $1 < x/d_1 < 7$, $L_{xy,min}$ gradually decreased until $L_{xy,min} = 0.15$ m. In the second half of the roller, $L_{xy,min}$ presented a stronger decrease representing low interaction in the large longitudinal free-surface structures at the end of the roller. Large differences were observed between L_{xy} calculated with constant integration limits and $L_{xy,min}$. The length scale estimation presented values of $L_{xy,min} > 2 \times L_{xy}$ near the jump toe. Further downstream, for $x/d_1 \geq 15$, $L_{xy,min}$ tended to similar values as L_{xy} calculated with $\Delta x_{max} = 0.23$. Further research is needed to identify the differences with previous instruments, the effect of inflow conditions and filtering of the raw data.

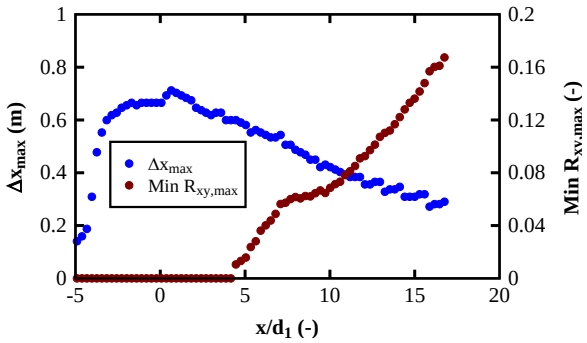

a) Minimum cross-correlation values $R_{xy,min}$ and corresponding integration distance Δx_{max}

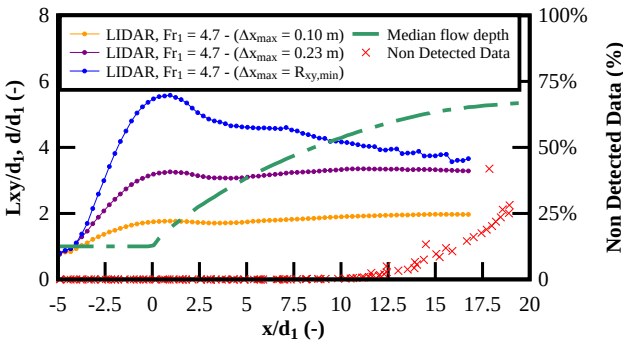

b) Comparison of L_{xy} and $L_{xy,min}$ along the hydraulic jump

Figure 8. Effect of lower integration limit $R_{xy,min}$ and integration distance Δx_{max} on the free-surface integral length scales.

6. Conclusions

This paper presented the measurements of the free-surface characteristics in an aerated hydraulic jump with a LIDAR. The free-surface characteristics were evaluated for a freely moving fully aerated hydraulic jump. Slight differences between the mean and median profiles were observed near the jump toe highlighting the effect of the jump toe oscillations on the free-surface features. Auto- and cross-correlation analyses of the free-surface data were performed and the integral free-surface turbulent time and length scales were calculated. Large auto-correlation time scales were observed close to the jump toe ($T_{xx} = 0.25$s). Towards the downstream end of the hydraulic jump, the free-surface time scales were similar to the auto-correlation time scales observed in air-water flows. The cross-correlation time scales were of similar order of magnitude to the auto-correlation time scales decreasing in magnitude with increasing distance between points of cross-correlation. Good agreement was found in the maximum cross-correlation coefficients $R_{xy,max}$ between the present LIDAR data and previous studies showing an exponential decay along the hydraulic jump. The LIDAR data provided continuous integral free-surface length scales. While the turbulent length scales were of similar magnitude compared to previous studies, the present integral turbulent lengths scales were larger in particular in the region close to the jump toe. This may be linked with the oscillations of the jump toe which were included in the present analysis. The estimation of the turbulent length scales was also strongly affected by the lower integration limit and the present study used the minimum value of $R_{xy,max}$ as the lower integration limit. Further research is needed to compare the LIDAR observations of the free-surface features with simultaneously sampled instrumentation which has been used in previous studies. Previous studies also used low and high pass filtering of the raw signals and any filtering effects on the integral free-surface time and length scales should be investigated.

7. Acknowledgements

The authors thank Rob Jenkins and Larry Paice from UNSW Water Research Laboratory for their technical support.

8. References

Bakhmeteff, B. A., and Matzke, A. E. (1936). "The hydraulic jump in terms of dynamic similarity". In Proceedings of the *American Society of Civil Engineers*, 61(2) 145-162.

Blenkinsopp, C. E., Turner, I. L., Allis, M. J., Peirson, W. L., and Garden, L. E. (2012). "Application of LiDAR technology for measurement of time-varying free-surface profiles in a laboratory wave flume." *Coastal Engineering*, 68, 1-5.

Chachereau, Y., and Chanson, H. (2010) "Free-surface turbulent fluctuations and air–water flow measurements in hydraulics jumps with small inflow Froude numbers." Hydraulic Model Report No. CH78/10, School of Civil Engineering, The University of Queensland, Brisbane, Australia, 133 pages.

Chachereau, Y., and Chanson, H. (2011). "Free-surface fluctuations and turbulence in hydraulic jumps." *Experimental Thermal and Fluid Science*, 35(6), 896-909.

Damiani, L., and Valentini, N. (2014). "Terrestrial Laser Scanner as a measurement instrument for laboratory water waves." *Proc., 1st Workshop on the State of the Art and Challenges of Research Efforts at Politecnico di Bari*, Gangemi Editore, Bari, Italy, 111-116.

Hager, W.H. (1993). "Classical Hydraulic Jump: free surface profile." *Canadian Journal of Civil Engineering*, 20(3), 536-539.

Kucukali, S., and Chanson, H. (2008). "Turbulence measurements in the bubbly flow region of hydraulic jumps." *Experimental Thermal and Fluid Science*, 33(1), 41-53.

Li, R., Montano, L., and Felder, S. (2017). "LIDAR measurements of free-surface characteristics in a hydraulic jump". *Proc., 13th Hydraulics in Water Engineering Conference* (HIWE2017), 13-16 November 2017, Sydney, Australia, P. Brady and S. Felder Editors, Engineers Australia, 8 pages.

Montano, L., and Felder, S. (2017). "Measurements of air-water flow properties in hydraulic jumps in a sloping channel". *Proc., 13th Hydraulics in Water Engineering Conference* (HIWE2017), 13-16 November 2017, Sydney, Australia, P. Brady and S. Felder Editors, Engineers Australia, 9 pages.

Montano, L., Li, R., and Felder, S. (2018). "Continuous measurements of time-varying free-surface profiles in aerated hydraulic jumps with a LIDAR" *Experimental Thermal and Fluid Science*; doi.org/10.1016/j.expthermflusci.2018.01.016

Mouaze, D., Murzyn, F., and Chaplin, J.R. (2005). "Free surface length scale estimation in hydraulic jumps." *Journal of Fluids Engineering*, 127(6), 1191-1193.

Murzyn, F., and Chanson, H. (2009). "Free-surface fluctuations in hydraulic jumps: Experimental Observations." *Experimental Thermal and Fluid Science*, 33(7), 1055-1064.

Murzyn, F., Mouaze, D., and Chaplin, J.R. (2007). "Air-water interface dynamic and free surface features in hydraulic jumps." *Journal of Hydraulic Research*, 45(5), 679-685.

Rajaratnam, N. (1962). "Profile equation for the Hydraulic Jump." *Water Power*, 14, 324-327.

Rouse, H., Siao, T. T., and Nagaratnam, S. (1959). "Turbulence characteristics of the hydraulic jump." *Journal of the Hydraulics Division*, 84(1), 1-30.

Streicher, M., Hofland, B., and Lindenbergh, R. C. (2013). "Laser ranging for monitoring water waves in the new Deltares Delta Flume." *ISPRS.*

SICK (2015). Laser Measurement Sensors: Operating Instructions. Germany.

Wang, H. (2014). "Turbulence and air entrainment in hydraulic jumps." PhD Thesis. School of Civil Engineering. University of Queensland, Australia, 341 pages.

Wang, H., Felder, S., and Chanson, H, (2014). 'An experimental study of turbulent two-phase flow in hydraulic jumps and application of a triple decomposition technique', Experiments in Fluids, 55, 1 – 18.

Wang, H., and Chanson, H. (2015). "Experimental study of turbulent fluctuations in hydraulic jumps." *Journal of Hydraulic Engineering*, 174(7), Paper 04015010, 10 pages.

Wang, H., and Murzyn, F. (2016). "Experimental assessment of characteristic turbulent scales in two-phase flow of hydraulic jump: from bottom to free surface." *Environmental Fluid Mechanics*, 17(1), 7 – 25.